The response of clamped sandwich plates with metallic foam cores to simulated blast loading

D.D. Radford, G.J. McShane, V.S. Deshpande and N.A. Fleck*

Department of Engineering, University of Cambridge

Trumpington St., Cambridge, CB2 1PZ, UK

Abstract

The dynamic responses of clamped circular monolithic and sandwich plates of equal areal mass have been measured by loading the plates at mid-span with metal foam projectiles. The sandwich plates comprise AISI 304 stainless steel face sheets and aluminium alloy metal foam cores. The resistance to shock loading is quantified by the permanent transverse deflection at mid-span of the plates as a function of projectile momentum. It is found that the sandwich plates have a higher shock resistance than monolithic plates of equal mass. Further, the shock resistance of the sandwich plates increases with increasing thickness of sandwich core. Finite element simulations of these experiments are in good agreement with the experimental measurements and demonstrate that the strain rate sensitivity of AISI 304 stainless steel plays a significant role in increasing the shock resistance of the monolithic and sandwich plates. Finally, the finite element simulations were employed to determine the pressure versus time history exerted by the foam projectiles on the plates. It was found that the pressure transient was reasonably independent of the dynamic impedance of the plate, suggesting that the metal foam projectile is a convenient experimental tool for ranking the shock resistance of competing structures.

Keywords: impact loading, sandwich plates, metallic foams, finite elements

Revised version submitted to Int. J. Solids Structures, June 2005

* Corresponding author, Tel.: +44-1223 332650; fax: +44-1223 765046
Email address: naf1@eng.cam.ac.uk

1. Introduction

Clamped monolithic plates are commonly used in the design of commercial and military vehicles. For example, the outermost hull of a ship comprises plates welded to an array of stiffeners. The superior performance of sandwich plates relative to monolithic solid plates is well established for applications requiring high quasi-static strength. However, the resistance of sandwich plates to dynamic loads remains to be fully investigated in order to quantify the advantages of sandwich design over monolithic design for potential application in shock resistant structures.

Over the past fifty years, the response of monolithic beams and plates to shock type loading has been extensively investigated. For example, Wang and Hopkins (1954) and Symmonds (1954) have analysed the impulse response of clamped circular monolithic plates and clamped monolithic beams, respectively. Their analyses were restricted to infinitesimal strains and displacements. Jones (1968) presented an approximate analytical solution for the finite deflection of simply supported circular monolithic plates by direct application of the principle of virtual work for an assumed deformation mode. More recently, Fleck and Deshpande (2004) have proposed an analytical model for the finite deflection response of clamped sandwich beams subjected to shock loadings, including the effects of fluid-structure interaction. They have demonstrated the accuracy of their analytical model in the case of no fluid-structure interaction by direct comparison with the finite element calculations of Xue and Hutchinson (2004) for clamped sandwich beams. The analytical model of Fleck-Deshpande has been extended by Qiu et al. (2005) for clamped circular sandwich plates, and is again supported by finite element calculations of Xue and Hutchinson (2003) for sandwich plates with a foam-like core and the effects of fluid-structure interaction again neglected. These recent investigations have each demonstrated that circular sandwich plates can posses a superior resistance to shock loading than monolithic plates of the same areal mass.

To date, there have been little experimental data to support or refute these predictions, as it is difficult to perform laboratory scale experiments with a prescribed dynamic loading history. In the recent study by Radford et al. (2005a), an experimental technique was introduced to subject structures to high intensity pressure pulses using metal foam

projectiles. The applied pressure versus time pulse attempts to mimic shock loading in air and in water, with peak pressures on the order of 100 MPa and loading times of approximately 100 μs. This experimental technique has been employed by Radford et al. (2005b) and Rathbun et al. (2004) to investigate the dynamic response of clamped sandwich beams with metal foam and lattice cores. These studies indicated that the sandwich beams have a superior shock resistance compared to monolithic beams of the same mass. However, no attempt was made to de-convolute the cross-coupling between the dynamic response of the beams and that of the projectile, making it difficult to quantify the enhanced shock resistance of the sandwich beams.

In this study, we employ the experimental technique of Radford et al. (2005a) to explore the shock resistance of clamped circular monolithic and aluminium foam core sandwich plates of equal mass. First, the manufacturing route of the sandwich plates is detailed and the experimental procedure is described for loading the plates at mid-span by metal foam projectiles. The experimental results are compared with finite element predictions. Finally, the finite element simulations are used to determine the cross-coupling between the foam projectile loading and the plate response.

2. Experimental investigation

In this study, metal foam projectiles are used to load dynamically clamped circular sandwich plates comprising an aluminium metal foam core and AISI 304 stainless steel face sheets. The main aims of the experimental investigation are:

(i) To compare the dynamic resistance of sandwich plates with monolithic plates (made from the sandwich plate face sheet material) of equal mass.
(ii) To investigate the effect of the sandwich core thickness upon the shock resistance.
(iii) To demonstrate the accuracy of finite element predictions for the dynamic response.

2.1 Specimen configuration and manufacture

Circular sandwich plates comprising Alporas[1] aluminium metal foam cores and AISI type 304 stainless steel face sheets were manufactured to a net areal mass m of 23.5 kgm^{-2}. The plates, of radius $R = 80$ mm, comprised two identical AISI 304 stainless steel face sheets, of thickness h and density $\rho_f = 8060$ kgm^{-3}, and an Alporas aluminium foam core, of density $\rho_c \approx 430$ kgm^{-3} and thickness c, see Fig. 1. In order to achieve a common areal mass of $m = 2h\rho_f + c\rho_c = 23.5$ kgm^{-2}, face sheets of thickness $h = 1.18$ mm and 0.88 mm were employed for cores of thickness $c = 10$ mm and 22 mm, respectively.

The sandwich plates were manufactured as follows. Alporas foam cores of rectilinear dimension $250\text{ mm} \times 250\text{ mm} \times c$ were electro-discharged machined from blocks of foam. Stainless steel face sheets of dimensions $250\text{ mm} \times 250\text{ mm} \times h$ were degreased and abraded, and were then adhered to the foam core using Redux 322 epoxy adhesive on a nylon carrier mesh. The sandwich plates were air-cured at 175^{o}C for 1.5 hours, and bonding was facilitated by imposing dead-loading with a nominal contact pressure of 0.01 MPa. Finally, eight equally spaced clearance holes for M8 bolts were drilled in these plates on a pitch circle of radius 102 mm.

The clamped plate geometry is sketched in Fig. 2. Each sandwich plate was clamped between two annular steel rings of thickness 7 mm, inner radius 80 mm and outer radius 125 mm, on a pitch circle of radius 102 mm. The assembly was then bolted down onto a rigid loading frame by M8 bolts, as sketched in Fig. 2.

In addition to the dynamic tests on two configurations of sandwich plates, dynamic tests were performed on AISI 304 stainless steel monolithic circular plates of areal mass m=23.5 kgm^{-2} for comparison purposes. These circular monolithic plates of radius $R = 80$ mm and thickness $h = 2.92$ mm were gripped using the same apparatus as that described above.

[1] Shinko Wire Co. Ltd., Amagasaki, Japan.

2.2 Properties of the constituent materials

The uniaxial compressive responses of the Alporas metal foam was measured quasi-statically at a nominal strain rate of 0.001 s^{-1} using two sizes of cuboidal specimens, with a side-length $L = 10$ mm and 22 mm. These lengths correspond to the two core thicknesses employed in the sandwich tests. The measured compressive nominal stress versus nominal strain responses are plotted in Fig. 3a. The overall responses of the two cores are similar, with a compressive plateau strength of 3.5 MPa and a nominal lock-up strain ε_D of 0.8. The uniaxial tensile responses of the three thicknesses of AISI 304 stainless steel used in the sandwich and monolithic plates were measured at a nominal strain rate of 0.001 s^{-1}, and the true tensile stress versus logarithmic strain curves are plotted in Fig. 3b. The tensile responses of the three thicknesses of AISI 304 stainless steel are qualitatively similar with a 0.2% offset yield strength of 300 MPa, followed by a linear hardening response up to an ultimate tensile strength of 1150 MPa.

The sandwich panels made from the Alporas metal foam and AISI 304 stainless steel face sheets were tested under dynamic loading and thus a knowledge of the high strain rate behaviour of the metal foams and AISI 304 stainless steel is necessary for accurate finite element simulations of the experiments. While the Alporas metal foam has a small strain rate sensitivity (Dannemann and Lankford, 2000 and Miyoshi et al., 2002), shock wave propagation in these foams becomes important at impact velocities exceeding about 50 ms^{-1} (Radford et al. 2005a). The algorithm employed in the finite element simulations to capture the strain rate and shock wave effects are given in Section 4, with additional details given in Appendix A.

Stout and Follansbee (1986) have investigated the strain rate sensitivity of AISI 304 stainless steel for strain rates in the range 10^{-4} $s^{-1} < \dot{\varepsilon} < 10^{4}$ s^{-1} by performing a series of compression tests. In order to present their results, we introduce the strength enhancement ratio *R* as the ratio of the stress $\sigma_d(\varepsilon^p = 0.1)$ at any applied strain rate $\dot{\varepsilon}^p$ to the reference stress $\sigma_0(\varepsilon^p = 0.1)$ at an applied $\dot{\varepsilon}^p = 10^{-3}$ s^{-1}. Their data for AISI 304 stainless steel is re-plotted in Fig. 4 in the form of *R* versus the plastic strain rate $\dot{\varepsilon}^p$ for $10^{-4}\,s^{-1} < \dot{\varepsilon}_p < 10^{4}\,s^{-1}$. The strength enhancement ratio *R* is reasonably independent of the

choice of the plastic strain ε^p at which R is calculated. Thus, the dynamic strength σ_d versus plastic strain ε^p history can be expressed as

$$\sigma_d(\varepsilon^p)=R(\dot{\varepsilon}^p)\sigma_0(\varepsilon^p) \ , \qquad (1)$$

where $R(\dot{\varepsilon}^p)$ is given in Fig. 4a. In the finite element simulations of the dynamic response of the sandwich panels presented in Section 4, we shall employ this prescription for the strain rate sensitivity of the AISI 304 stainless steel, with $\sigma_0(\varepsilon^p)$ given by the measured quasi-static stress versus strain histories for the various thicknesses of AISI 304 stainless steel (Fig. 3b). As an example, the estimated true tensile stress versus logarithmic plastic strain histories for the 1.18 mm thick AISI 304 stainless steel at four selected values of applied strain rate are sketched in Fig. 4b.

2.3 Test protocol

Alporas aluminium foam projectiles were used to impact the clamped monolithic and sandwich plates over a central circular patch of radius *a*, as shown in Fig. 1. The use of foam projectiles as a means of providing well-characterised pressure versus time has recently been developed by Radford et al. (2005a) and then subsequently employed by Radford et al. (2005b) to investigate the dynamic response of clamped sandwich beams with metal foam cores and with lattice cores.

Circular cylindrical projectiles of length $l_0 \approx 50$ mm and diameter $d = 28.5$ mm were electro-discharge machined from Alporas foam blocks of density ρ_p in the range 380 kgm^{-3} to 490 kgm^{-3}. The projectiles were fired from a gas gun of barrel diameter 28.5 mm and length 4.5 m. The projectile velocities v_0 ranged from 160 ms^{-1} to 570 ms^{-1}, providing a projectile momentum per unit area $I_0 = \rho_p l_0 v_0$ of up to 13 kNs m^{-2}. Table 1 summarises the set of experiments performed, with details of the projectile density, length, impact velocity and initial momentum. The plates were examined after each test to measure the permanent deflection of the faces, and to detect any visible signs of failure.

3. Experimental results

For each specimen configuration, at least four levels of initial momentum were applied by varying the density, length and impact velocity of the foam projectiles. Table 1 summarises the observed permanent back-face transverse deflection at the mid-span and the amount of core compression for each specimen.

The effect of core thickness upon the shock resistance is summarised in Fig. 5. It contains a plot of the permanent back-face deflection at mid-span versus the momentum of the foam projectile I_0. The plate of core thickness $c = 22$ mm deflects less than the sandwich plate of core thickness $c = 10$ mm over the entire range of I_0 investigated. The mid-span deflections of the monolithic plates of equal areal mass are included in Fig. 5. Intriguingly, the monolithic plate deflects less than the sandwich plates at low values of I_0.

The final core compressive strain is defined as $\varepsilon_c = \Delta c / c$, where Δc is the reduction in core thickness at mid-span; the measured dependence of the ε_c upon I_0 is given in Fig. 6 for the two sandwich plate configurations. The core compressive strain increases with increasing I_0, and is consistently less for the thicker core. At the highest impulse ($I_0 \approx 13$ kNs m^{-2}), both sandwich plates have fully compressed such that the lock-up strain of the metal foam core has been achieved at mid-span.

In order to gain insight into the dynamic deformation mechanisms, the monolithic and sandwich plates tested at $I_0 \approx 13$ kNs m^{-2} were sectioned along their diametral planes. Photographs of the diametral sections are shown in Fig. 7a for the monolithic plate (specimen M9, back-face deflection of 14.2 mm), in Fig.7b for the sandwich plate of core thickness 10 mm (specimen A4, back-face deflection of 12.8 mm) and in Fig.7c for the sandwich plate of core thickness 22 mm (specimen B4, back-face deflection of 9.2 mm). The diametral profiles show that significant plastic deformation occurred in the vicinity of the foam impact and that the plates are continuously curved. This suggests that the dynamic deformation of plates involves the formation of travelling hinges, analogous to the behaviour of monolithic and sandwich beams (Radford et al. 2005b). Delamination of the core from the face sheets is evident in Fig. 7c; it occurred after the specimen was sectioned, rather than during the impact experiment.

For comparison purposes, a clamped monolithic plate and the two configurations of sandwich plates were loaded quasi-statically over a central patch. These experiments were performed at a displacement rate of 10^{-5} ms^{-1} using a flat-bottomed steel cylindrical punch, of diameter 28.5 mm. The specimens were loaded until the back-face deflection at mid-span matched that in the dynamic experiments (Fig. 7). Upon unloading the specimens were sectioned along their diametral planes. The photographs shown in Fig. 8 reveal membrane action, with stationary plastic hinges at the periphery of the indenter and at the supports (as evidenced by the discontinuity in inclination of the plates at those locations).

4. Finite element simulations

Comparisons of the finite element (FE) simulations and the measured responses of the monolithic and sandwich plates are presented in this section. All computations were performed using the explicit time integration version of the commercially available finite element code ABAQUS[2] (version 6.4). The circular plates were modelled using four noded axisymmetric quadrilateral elements with reduced integration (*CAX4R* in ABAQUS notation). Clamped boundary conditions, with vanishing displacements in the radial and tangential directions, were prescribed on the outer radius of the plate, $r = R$. Dynamic loading of each plate was simulated by impact of a foam projectile, as described subsequently. Typically, there were 160 elements along the radius of each plate and approximately three elements per millimetre through the thickness of the face sheets. The prescription employed to set the mesh density in the foam core (and foam projectile) is given in Appendix A. Mesh sensitivity studies revealed that further refinements did not appreciably improve the accuracy of the calculations.

The cylindrical foam projectiles of diameter 28.5 mm were also modelled using *CAX4R* axisymmetric elements, with contact between the outer surface of the projectile and the top surface of the plates modelled by a frictionless contact surface as provided by ABAQUS. At the start of the simulation, the projectile was imparted with a uniform initial velocity v_o and was brought into contact with the plate at its mid-span.

4.1 Constitutive description

The AISI 304 stainless steel face sheets of the sandwich plates were modelled by J2-flow theory rate dependent solids of density $\rho_f = 8060$ kgm^{-3}, Young's modulus $E = 210$ GPa and Poisson ratio $\nu = 0.3$. The uniaxial tensile true stress versus equivalent plastic strain curves at plastic strain rates 10^{-3} s^{-1} $\leq \dot{\varepsilon}^p \leq$ 10^4 s^{-1} were tabulated in ABAQUS using the prescription described in Section 2.2. Reference calculations were also performed, with the rate dependence of the AISI 304 stainless steel neglected by setting $R(\dot{\varepsilon}^p)$ =1 in equation (1). Thus, these rate independent calculations made direct use of the quasi-static tensile stress versus strain response of the AISI 304 stainless steels (Fig. 3b).

The foam core and the projectile were modelled as a compressible continuum using the metal foam constitutive model of Deshpande and Fleck (2000). Write s_{ij} as the usual deviatoric stress and the von Mises effective stress as $\sigma_e \equiv \sqrt{3 s_{ij} s_{ij} / 2}$. The isotropic yield surface for the metal foam is specified by

$$\hat{\sigma} - Y = 0, \tag{2}$$

where the equivalent stress $\hat{\sigma}$ is a homogeneous function of σ_e and mean stress $\sigma_m \equiv \sigma_{kk} / 3$ according to

$$\hat{\sigma}^2 \equiv \frac{1}{1 + (\alpha / 3)^2} \left[\sigma_e^2 + \alpha^2 \sigma_m^2 \right]. \tag{3}$$

The material parameter α denotes the ratio of deviatoric strength to hydrostatic strength, and the normalisation factor on the right hand side of relation (3) is chosen such that $\hat{\sigma}$ denotes the stress in a uniaxial tension of compression test. An over-stress model is employed with the yield stress Y specified by

$$Y = \eta \dot{\hat{\varepsilon}}^p + \sigma_c, \tag{4}$$

---

[2] Hibbit, Karlsson and Sorensen Inc.

where η is the viscosity, $\dot{\hat{\varepsilon}}^p$ the plastic strain rate (work conjugate to $\hat{\sigma}$), and $\sigma_c(\hat{\varepsilon}^p)$ is the static uniaxial stress versus plastic strain relation. Normality of plastic flow is assumed, and this implies that the "plastic Poisson's ratio" $\nu_p = -\dot{\varepsilon}_{22}^p / \dot{\varepsilon}_{11}^p$ for uniaxial compression in the 1-direction is given by

$$\nu_p = \frac{1/2 - (\alpha/3)^2}{1 + (\alpha/3)^2} \tag{5}$$

In the simulations, the Alporas foam is assumed to have a Young's modulus $E_c = 1.0$ GPa, an elastic Poisson's ratio $\nu = 0.3$ and a plastic Poisson's ratio $\nu_p = 0$ (Ashby et al. 2000). The static yield strength σ_c versus equivalent plastic strain $\hat{\varepsilon}^p$ history is calibrated using the compressive stress versus strain responses presented in Fig. 3a. Data from the 22 mm thick foam specimen is used for the foam cores of thickness $c = 22$ mm and for the projectiles, while data from the 10 mm thick specimen is employed to model the foam core of thickness $c = 10$ mm. A prescription for the viscosity η is given in Appendix A.

The geometries of the simulated monolithic and sandwich plates match those of the experiments (cf. Section 2.1), with the density of the sandwich cores taken to be $\rho_c = 432$ kgm^{-3} and 428 kgm^{-3}, for the sandwich plates of core thickness $c = 22$ mm and 10 mm, respectively. The density and length of the foam projectiles are as listed in Table 1.

4.2 Comparison of finite element predictions and measurements

Unless otherwise stated, all calculations reported in this study have been performed with the rate dependent constitutive response for the AISI 304 stainless steel. Sample FE predictions of the mid-span deflection versus time histories of the monolithic plate specimen M9 and the sandwich plate specimen B4 ($c = 22$ mm) are plotted in Fig. 9, with I_0 =13 kN s m^{-2} in both cases. The figure shows the mid-span deflection of the back-face of the monolithic plate and of both front and back faces of the sandwich plate. The deflection time histories indicate that only small elastic vibrations occur after the peak

deflection has been attained. Moreover, the peak deflection is approximately equal to the final permanent deflection for both the monolithic and sandwich plates.

The predicted and measured mid-span, back-face deflections of the monolithic plates are shown in Fig. 10. The predictions are given for both the rate dependent and rate independent constitutive descriptions of the AISI 304 stainless steel. The permanent deflections in the FE calculations are estimated by averaging the displacements near the end of the calculations (over the time interval $t =$ 1.5 ms to 3.0 ms). It is concluded that the rate dependent FE model predicts the permanent deflection to reasonable accuracy, with a slight over-prediction at high values of I_0. On the other hand, the rate independent model substantially over-predicts the experimental measurements, especially for high I_0.

Similar comparisons of the predicted and measured permanent mid-span deflections are shown in Fig. 11 for the back-face of the sandwich plates. Again, good agreement between the rate dependent FE predictions and the measurements is seen. The FE predictions of the final core compression ε_c have been included in Fig. 6; these predictions assume the rate dependent model for the AISI 304 face sheets. The FE simulations predict the measurements with reasonable accuracy, but give a slight over-prediction of ε_c at low I_0.

4.3 Pressure versus time histories exerted by foam projectiles

The pressure versus time history exerted by the foam projectile on a structure depends upon the foam projectile (i) density ρ_p, (ii) length l_o, (iii) compressive stress versus strain response of the foam, and (iv) projectile velocity v_o (Radford et al. 2005a). The analysis of Radford et al. (2005a) suggests that metal foam projectiles exert a rectangular pressure versus time pulse of magnitude

$$p_0 = \sigma_c + \frac{\rho_p v_0^2}{\varepsilon_D}, \tag{6}$$

and duration

$$\tau = \frac{l_o \varepsilon_D}{v_o}, \tag{7}$$

on a rigid stationary target. Here, σ_c and ε_D are the plateau stress and nominal densification strain of the foam, respectively. This pressure versus time history, however, is sensitive to the structural response of the target: a decrease in the mechanical impedance of the target leads to a decrease in the applied pressure and to an increase in the pulse duration. Thus, it is unclear whether the observed differences in response of the various monolithic and sandwich plates for a given I_0 are due to differences in their intrinsic impact resistance, or a result of the application of different pressure time histories on the plates. We shall employ the FE calculations to clarify this ambiguity.

The pressure versus time history exerted by the foam projectile on the plates is derived from the FE simulations as

$$p(t) = \rho_p l_0 \dot{\bar{v}}(t), \tag{8}$$

where $\bar{v}(t)$ is the average axial velocity of the foam projectile at time t, and the over-dot denotes time differentiation. Momentum conservation implies that,

$$I_o = \int_0^\infty p(t)dt. \tag{9}$$

The accuracy of the pressure versus time histories, as extracted from the FE calculations using equation (8), was confirmed by performing additional FE calculations on the monolithic and sandwich plates with the pressure transients taken as the loading. Both the rate dependent and rate independent versions of the constitutive law for the AISI 304 face sheets were employed. In all cases, the deflections were within 0.5 % of those obtained previously using the projectile loading.

The calculated pressure versus time histories exerted by the foam projectiles on the monolithic plate M9, the sandwich plate A4 ($c = 10$ mm) and on the sandwich plate B4

($c = 22$ mm) are plotted in Fig. 12; in each case I_0 =13 kN s m^{-2}. (All FE calculations detailed here and subsequently have been performed using the strain rate sensitive model for the AISI 304 stainless steel.) While the differences between the pressure versus time histories are small, it is clear from Fig. 12 that the pressure pulse duration is shortest for the monolithic plate. Consequently, the average pressure exerted by the foam projectile on the monolithic plate is highest.

We quantify the effect of these differences in the pressure versus time histories upon the structural response of the plates in three steps. First, the pressure versus time histories exerted on the *sandwich* plates by the foam projectiles are extracted from the FE simulations using the above prescription. Second, the pressure versus time histories are applied to the *monolithic* plate on a central patch of diameter $d = 28.5$ mm, and the resulting mid-span deflection versus time history is recorded for a period of 3 ms. And third, the permanent mid-span deflection of the monolithic plate is evaluated from these deflection versus time histories.

FE predictions of the permanent back-face deflections at mid-span of the $c = 10$ mm sandwich plate and of the monolithic plate are plotted in Fig. 13a, each for the case of direct loading by the foam projectiles. Additionally, FE predictions are given for the mid-span deflection of the monolithic plates due to the pressure versus time loading history as exerted by the foam projectile on the *sandwich* plate; these predictions are labelled 'pressure loading'. Imposition of the pressure loading results in a slight reduction in the mid-span deflections of the monolithic plates, especially at large I_0. However, the overall conclusion that sandwich plates outperform monolithic plates at high values of I_0 remains unchanged. Similar comparisons of the FE predictions of the permanent back-face deflections at mid-span of the $c = 22$ mm sandwich plates and monolithic plates due to loading by foam projectiles are shown in Fig. 13b. Included in the figure are the associated permanent mid-span deflections of the monolithic plates loaded by the pressure versus time histories exerted by the foam projectile on the $c = 22$ mm sandwich plates. Again, the pressure loading results in a small reduction in the mid-span deflections of the monolithic plates at high values of I_0, but the overall conclusion that the $c = 22$ mm sandwich plates outperform the monolithic plates remains unchanged. We conclude that foam projectiles

are a convenient laboratory tool for investigating the dynamic response of such monolithic and sandwich plates.

5. Concluding remarks

Metal foam projectiles have been used to impact clamped circular plates of monolithic and sandwich construction, with a metal foam core. The permanent deflections, and core compression of the sandwich plates, have been measured as a function of the projectile momentum and the measured response are compared with finite element simulations. It is found that the deformation mode due to dynamic loading is significantly different to that observed in quasi-static loading, due in part to the occurrence of travelling plastic hinges in the dynamic case. The sandwich plates outperform monolithic plates of equal mass at sufficiently high values of projectile momentum. An increase in the core thickness (while keeping the areal mass fixed) enhances the shock resistance of the sandwich plates.

The finite element simulations capture the observed response with reasonable accuracy, and reveal that the strain rate sensitivity of the AISI 304 stainless steel plays a significant role in increasing the shock resistance of the monolithic and sandwich plates. It is shown explicitly that the pressure versus time history imparted on the clamped monolithic plates is similar to that imparted on the sandwich plates. Consequently, the structural response of the clamped plates is dictated mainly by the momentum of the foam projectile. The metal foam projectile is thereby a useful laboratory tool for exploring the shock resistance of monolithic and sandwich structures.

Acknowledgements

The authors are grateful to ONR for their financial support through US-ONR IFO grant number N00014-03-1-0283 on The Science and Design of Blast Resistant Sandwich Structures and to the Isaac Newton Trust, Trinity College Cambridge.

Appendix A: Prescription of the metal foam viscosity in the FE calculations

The prescription for choosing the viscosity η in the rate dependent metal foam constitutive law and the associated choice of the finite element mesh size e employed in the foam core and projectile are discussed in this Appendix.

Dynamic compression of a rate dependent foam gives rise to a shock wave of finite width as discussed in (Radford et al. 2005a). For a linear viscous foam, the shock width w is given by (Radford et al. 2005a)

$$w = \frac{\eta \varepsilon_D}{\rho \Delta v}, \qquad \text{(A1)}$$

where η is the linear viscosity, ρ the initial foam density, ε_D the nominal densification strain of the foam, and Δv the velocity jump across the shock. For the purposes of this discussion Δv is approximately equal to the projectile velocity v_o. In the finite element calculations, we choose η such that the shock width w is much less than the core thickness c of the sandwich and less than the projectile length l_o. This ensures that the viscosity η does not significantly affect the structural response.

Large gradients in stress and strain occur over the shock width w. To ensure that the finite element calculations resolve these large gradients accurately, the element size e in the core was taken to satisfy the condition $e \le w/10$.

References

Ashby, M. F., Evans, A. G., Fleck, N.F., Gibson, L.J., Hutchinson, J.W., Wadley, H. N. G., 2000. Metal Foams: A Design Guide. Butterworth-Heinemann, Oxford.

Dannemann, K. A., Lankford, J., 2000. High strain rate compression of closed-cell aluminium foams. Materials Science and Engineering: A **293(1-2)**: 157-164.

Deshpande, V. S., Fleck, N.A., 2000. Isotropic constitutive models for metallic foams. Journal of Mechanics and Physics of Solids **48**: 1253-1283.

Fleck, N. A. Deshpande, V.S., 2004. The resistance of clamped sandwich beams to shock loading. Journal of Applied Mechanics, ASME **71**(3): 386-401.

Jones, N., 1968. Impulsive loading of a simply supported circular rigid plate. Journal of Applied Mechanics **27**: 59.

Miyoshi, T., Mukai, T., Higashi, K., 2002. Energy absorption in closed-cell Al-Zn-Mg-Ca-Ti foam. Materials Transactions **43**(7): 1778-1781.

Qiu, X., Deshpande, V.S., Fleck, N.F., 2005. Impulsive loading over a central portion of clamped sandwich beams. Journal of Mechanics and Physics of Solids (in press).

Radford, D. D., Deshpande, V.S., Fleck, N.A., 2005a. The use of metal foam projectiles to simulate shock loading on a structure. International Journal of Impact Engineering (in press).

Radford, D. D., Fleck, N.A., Deshpande, V.S., 2005b. The response of clamped sandwich beams subjected to shock loading. International Journal of Impact Engineering (in press).

Rathbun, H. J., Radford, D.D., Xue, Z., Yang, J., Deshpande, V.S., Fleck, N.A., Hutchinson, J.W., Zok, F.W., Evans, A.G., 2004. A dynamic probe for validating simulations of shock loaded metallic sandwich panels. International Journal of Solids and Structures (submitted).

Stout, M. G. Follansbee, P.S., 1986. Strain rate sensitivity, strain hardening, and yield behavior of 304L stainless steel. Trans. ASME: Journal of Engineering Materials Technology **108**: 344-353.

Symmonds, P. S., 1954. Large plastic deformations of beams under blast type loading. Second US National Congress of Applied Mechanics.

Wang, A. J., Hopkins, H.G., 1954. On the plastic deformation of built-in circular plates under impulsive load. Journal of Mechanics and Physics of Solids **3**: 22-37.

Xue, Z., Hutchinson, J.W., 2003. Preliminary assessment of sandwich plates subject to blast loads. International Journal of Mechanical Sciences **45**: 687-705.

Xue, Z., Hutchinson, J.W., 2004. A comparative study of blast-resistant metal sandwich plates. International Journal of Impact Engineering **30**: 1283-1305.

Specimen	$I_o = \rho_p l_o v_o$ (kNsm^{-2})	ρ_p (kgm^{-3})	l_0 (mm)	v_0 (ms^{-1})	Mid-span deflection of back face (mm)	ε_C
M1	3.26	416	49	160	0.6	-
M2	3.69	371	49	205	1.3	-
M3	4.59	505	50	183	2.2	-
M4	6.12	457	49	271	4.0	-
M5	8.11	480	48	352	7.2	-
M6	8.97	457	49	400	8.2	-
M7	10.51	490	47	456	10.6	-
M8	11.75	493	48	496	12.2	-
M9	13.07	493	48	552	14.2	-
A1	3.26	433	47	160	2.0	0.07
A2	6.18	388	50	321	4.4	0.39
A3	9.93	509	45	434	8.1	0.71
A4	13.31	503	48	551	12.8	0.78
B1	3.15	393	51	157	1.1	0.05
B2	6.19	487	48	265	3.1	0.21
B3	9.54	490	47	414	5.7	0.48
B4	12.87	470	48	570	9.2*	0.81

Table 1: Summary of the dynamic experiments performed on circular monolithic and sandwich plates. The specimens labelled M denote monolithic plates, A denotes sandwich plates of core thickness c = 10 mm, and B denotes sandwich plates of core thickness c = 22 mm. The superscript * indicates that tensile failure of the front face occurred.

List of Figures

Figure 9. Finite element predictions of the mid-span deflection versus time histories of monolithic plate specimen M9 and $c = 22$ mm sandwich plate specimen B4. The figure shows the mid-span deflection of the back-face of the monolithic plate, and of both faces of the sandwich plate. $I_0 = 13$ kNs m^{-2}.

Figure 10. Measured and predicted back-face deflections for the monolithic plates.

Figure 11. Measured and predicted back-face deflections for the (a) $c = 10$ mm and (b) $c = 22$ mm sandwich plates.

Figure 12. The predicted pressure versus time histories exerted by the foam projectiles on the monolithic specimen M9, and the sandwich plate specimens A4 ($c = 10$ mm) and B4 ($c = 22$ mm). $I_0 = 13$ kNs m^{-2}.

Figure 13. Predicted back-face deflections at mid-span. (a) Sandwich plate ($c = 10$ mm) and monolithic plate loaded by projectile, and monolithic plate loaded by pressure transient; (b) Sandwich plate ($c = 22$ mm) and monolithic plate loaded by projectile, and monolithic plate loaded by pressure transient.

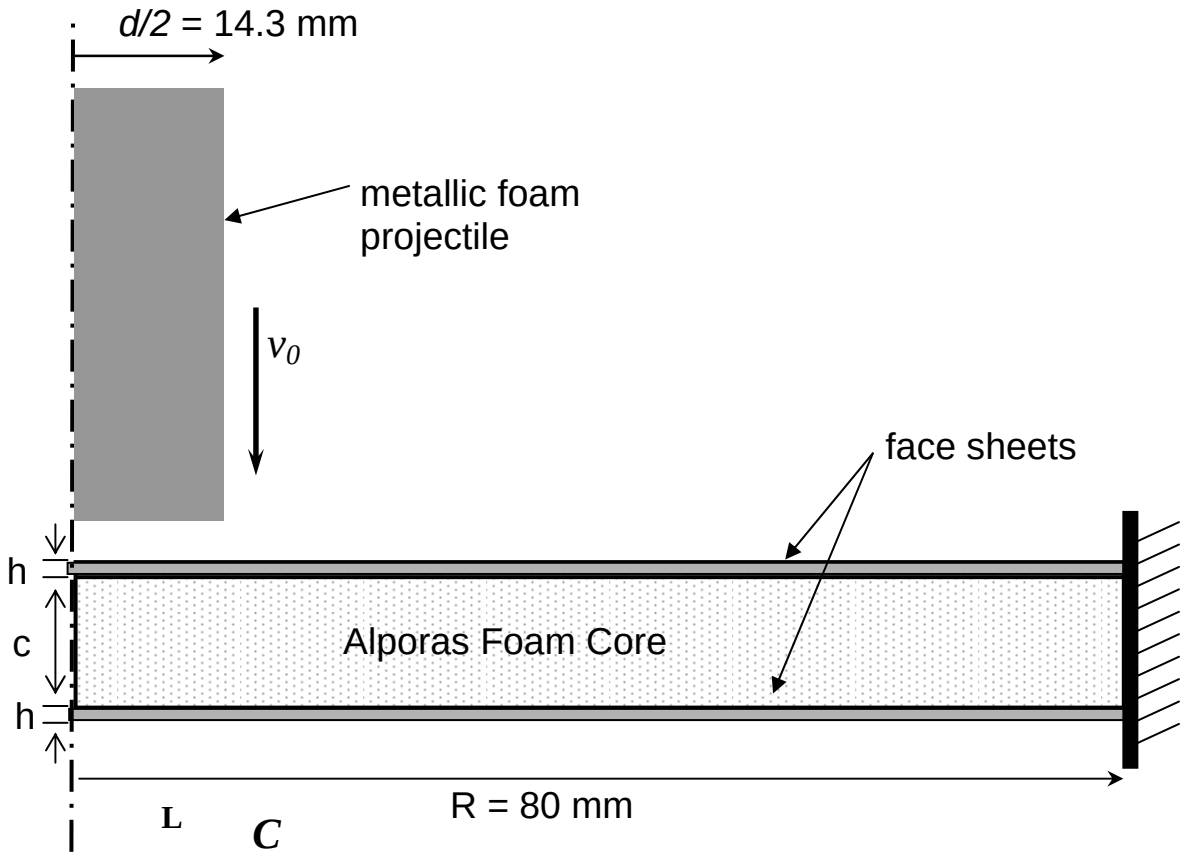

Figure 1: Sandwich plate geometry.

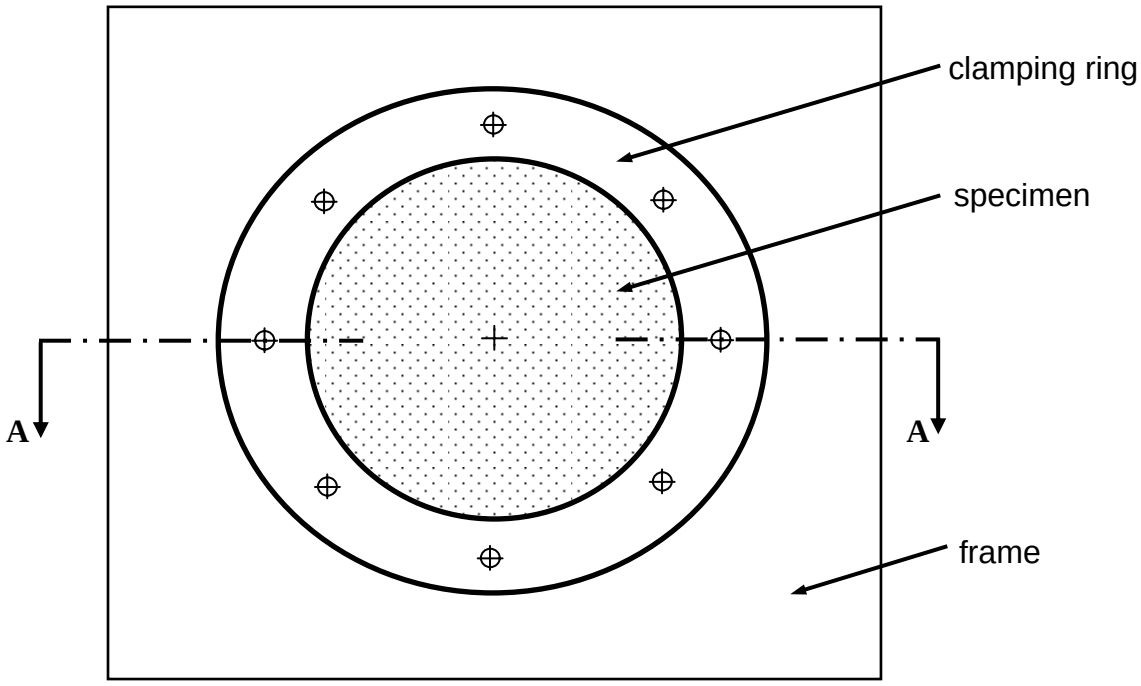

Plan View

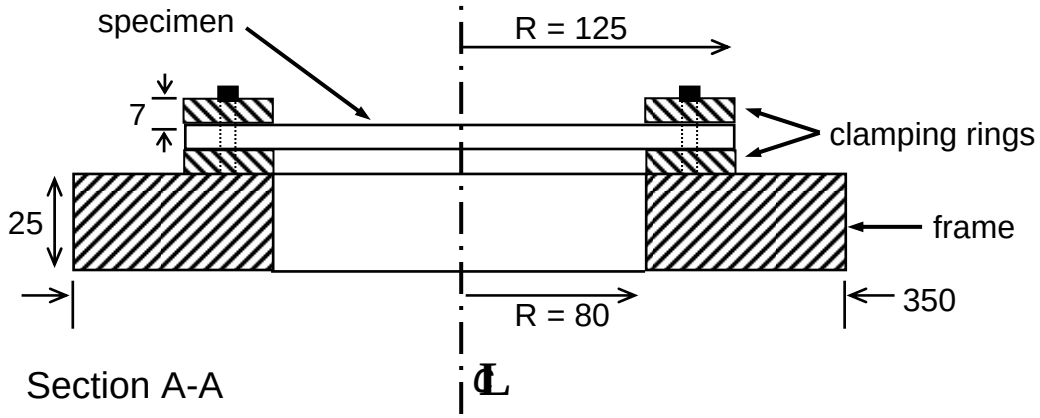

Figure 2: Sketch of the clamping arrangement. All dimensions are in mm.

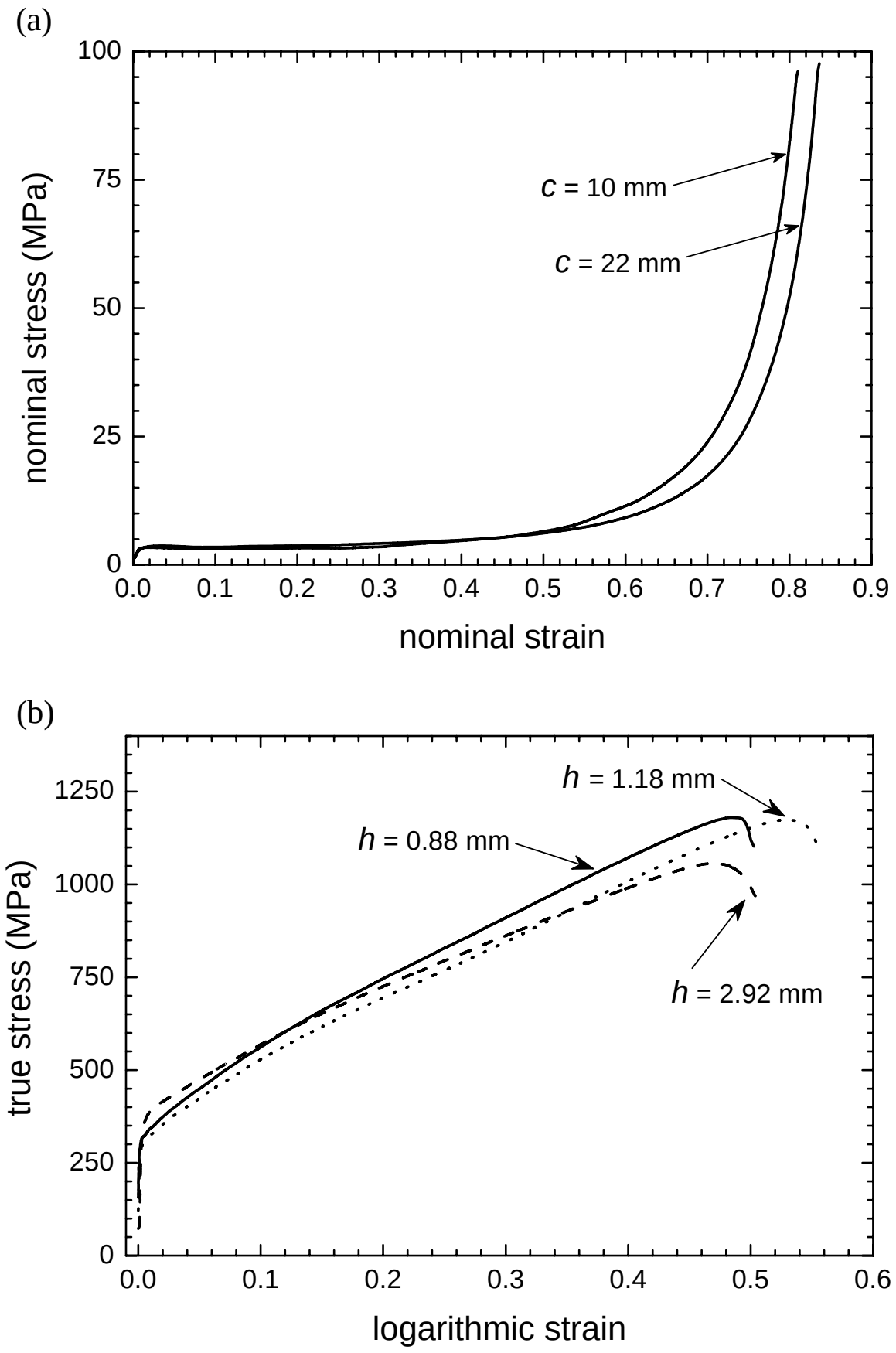

Figure 3. (a) Quasi-static compressive response for foam specimens of side-length L = 10 mm and 22 mm in the sandwich configuration; (b) Quasi-static tensile response of the AISI 304 stainless steel; results are shown for each sheet thickness, h.

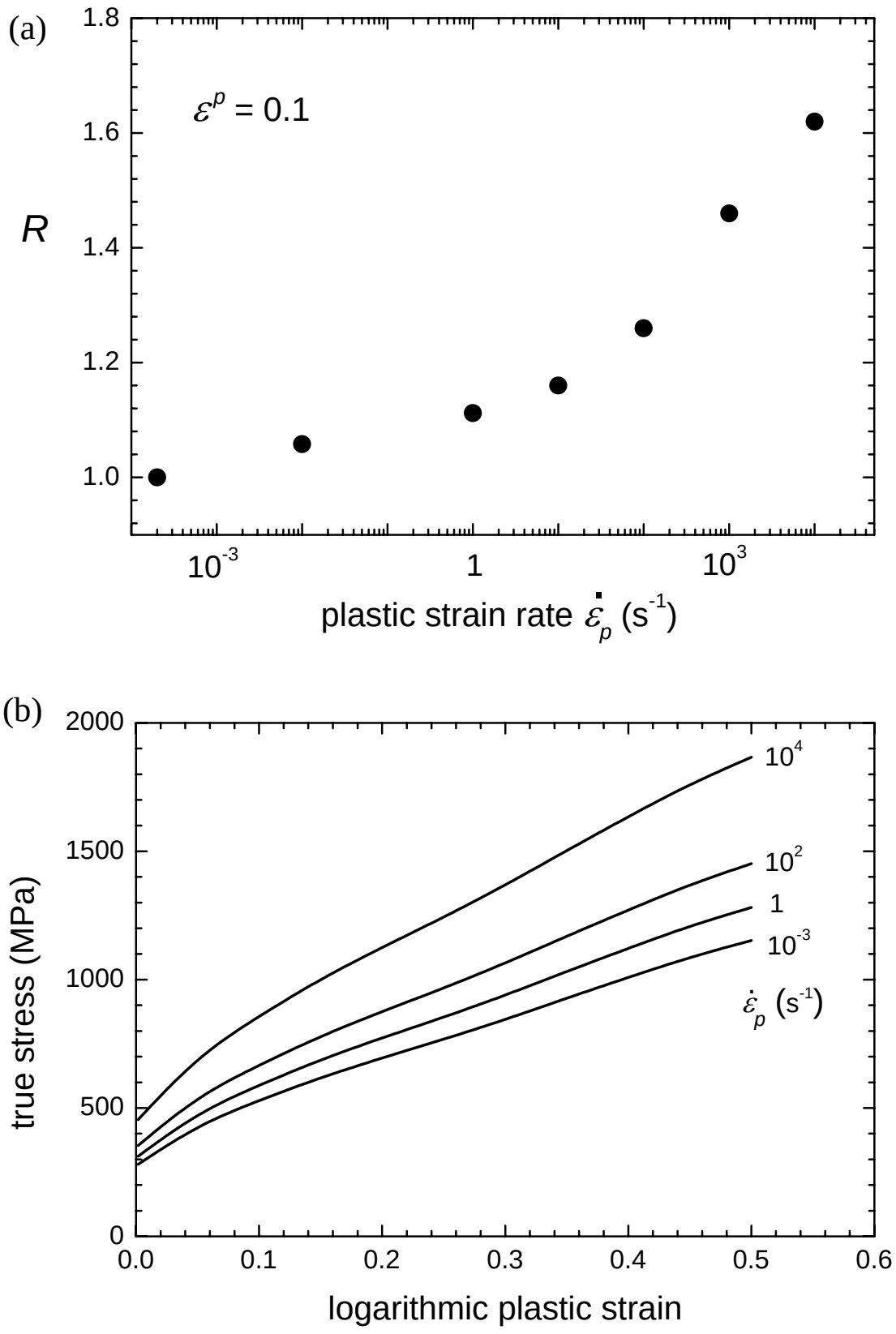

Figure 4. (a) The dynamic strength enhancement ratio R as a function of plastic strain rate $\dot{\varepsilon}^p$ for 304 stainless steel (Stout and Follansbee 1986). (b) Estimated tensile stress versus strain histories for 304 stainless steel (h = 1.18 mm) at three selected values of the applied strain rate.

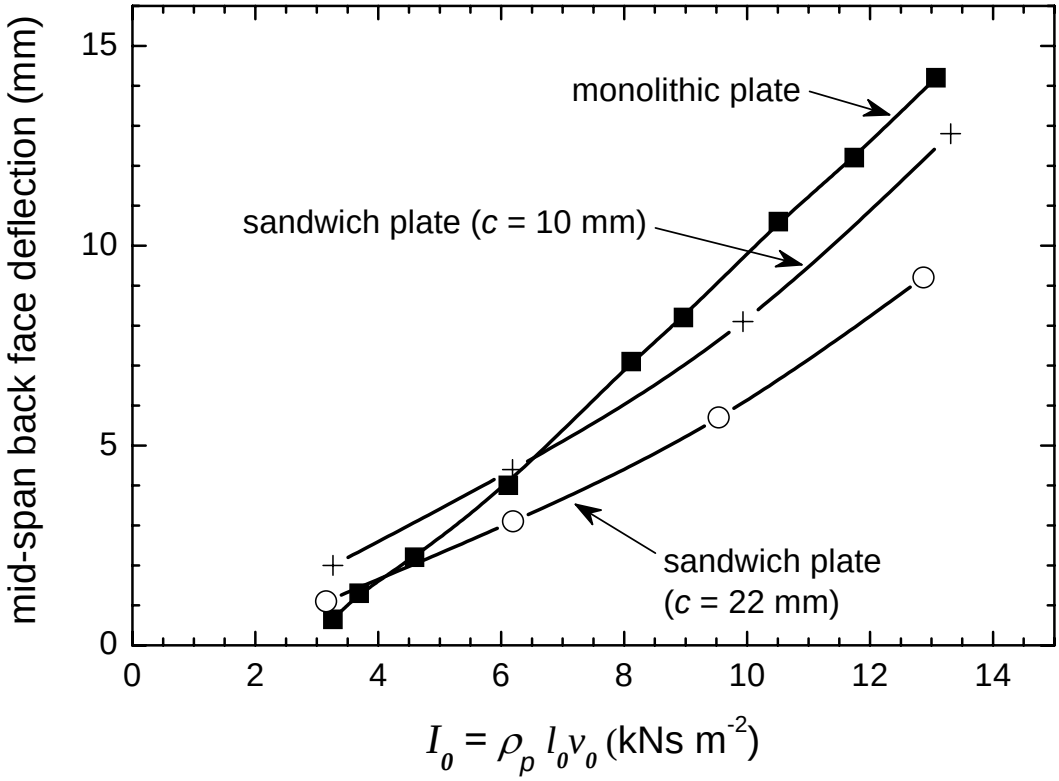

Figure 5. Measured permanent back-face deflection at mid-span of the dynamically loaded monolithic and sandwich plates, as a function of the initial foam projectile momentum I_0.

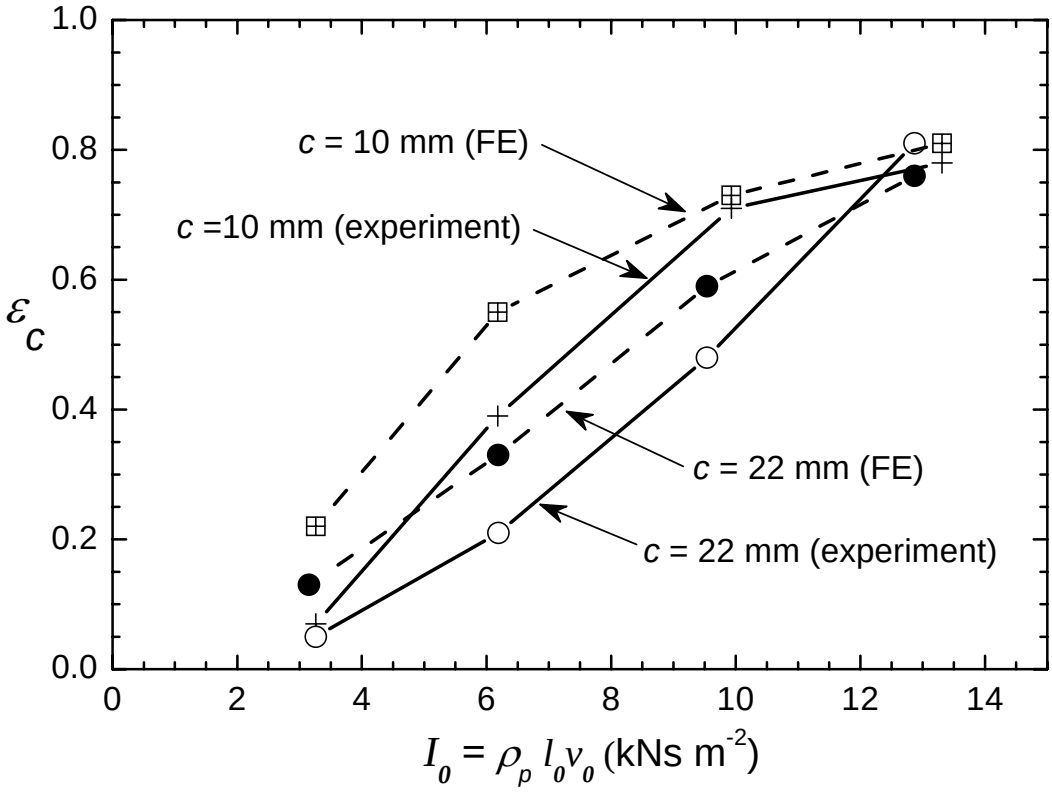

Figure 6. Measured permanent core compression ε_c at the mid-span of the dynamically loaded sandwich plates, as a function of the initial foam projectile momentum I_0. Finite element (FE) predictions (rate dependent model) for ε_c are included.

(a)

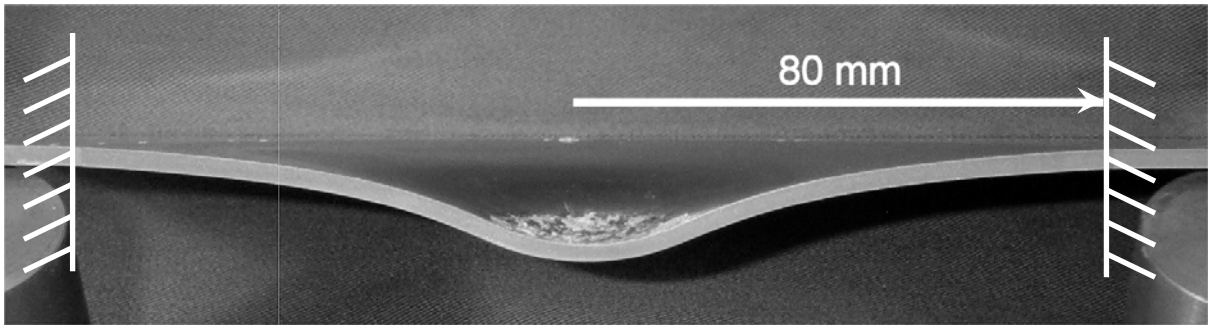

(b)

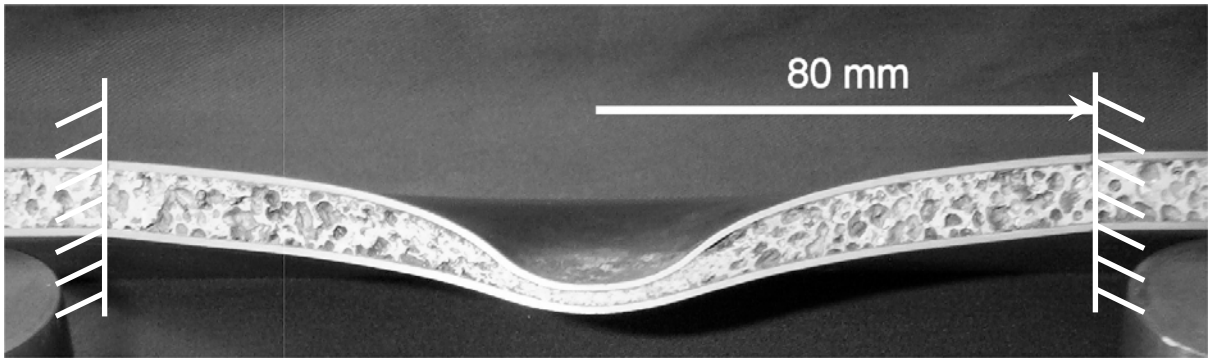

(c)

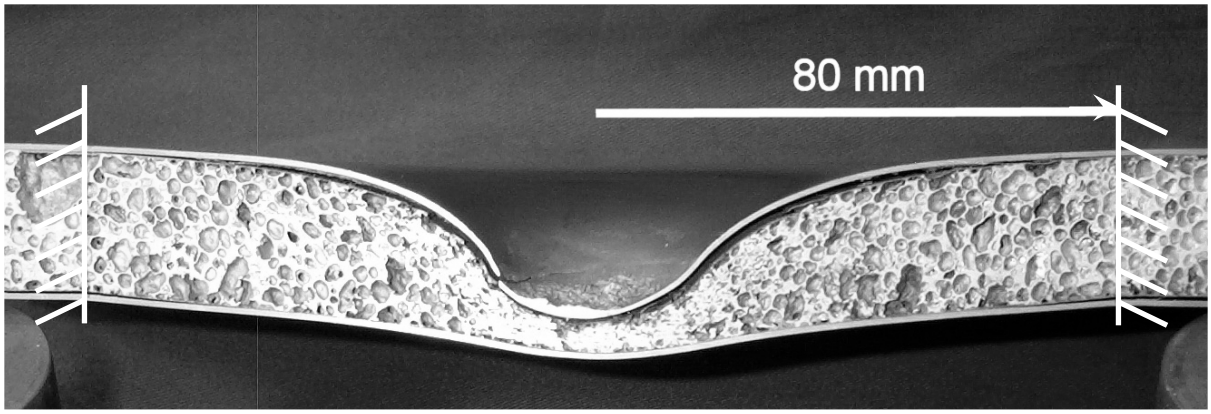

Figure 7. Photographs of the dynamically tested specimens (a) M9, (b) A4 and (c) B4. All these plates were tested at $I_0 = 13$ kNs m^{-2} and sectioned along their diametral plane.

(a)

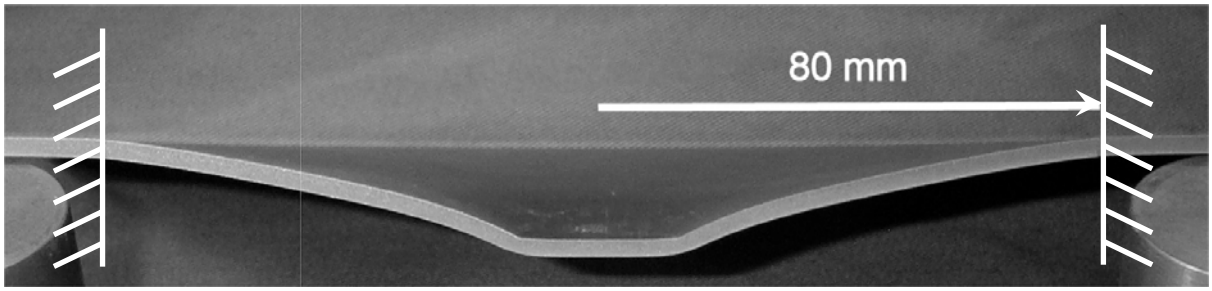

(b)

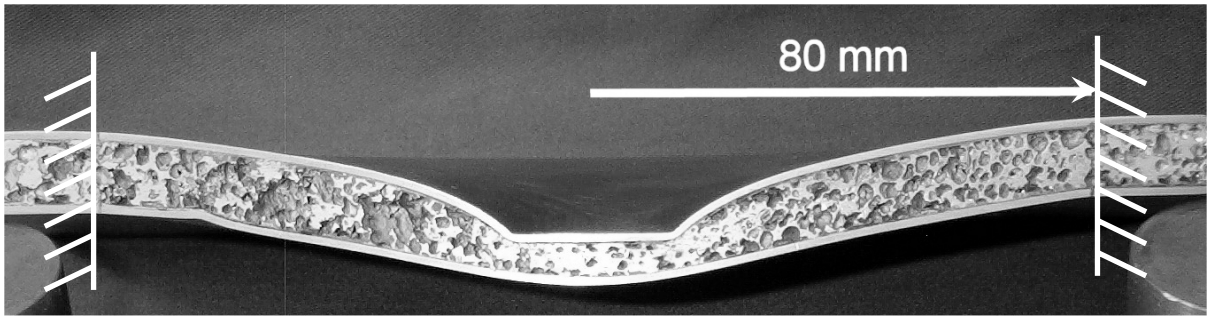

(c)

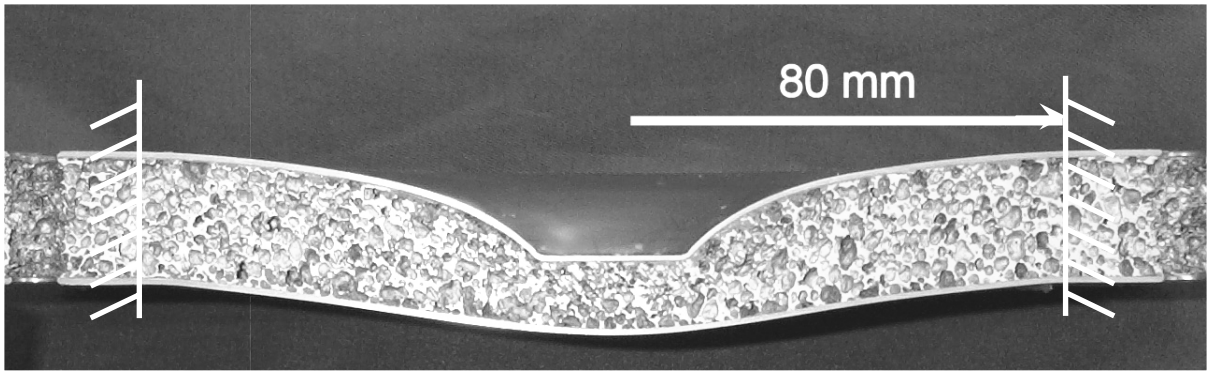

Figure 8. Photographs of the quasi-statically tested (a) monolithic plate (b) $c = 10$ mm sandwich plate and (c) $c = 22$ mm sandwich plate. These plates were loaded until the permanent back-face deflection at the mid-span matched that obtained in the corresponding dynamic experiments of Fig. 7 and sectioned along their diametral plane.

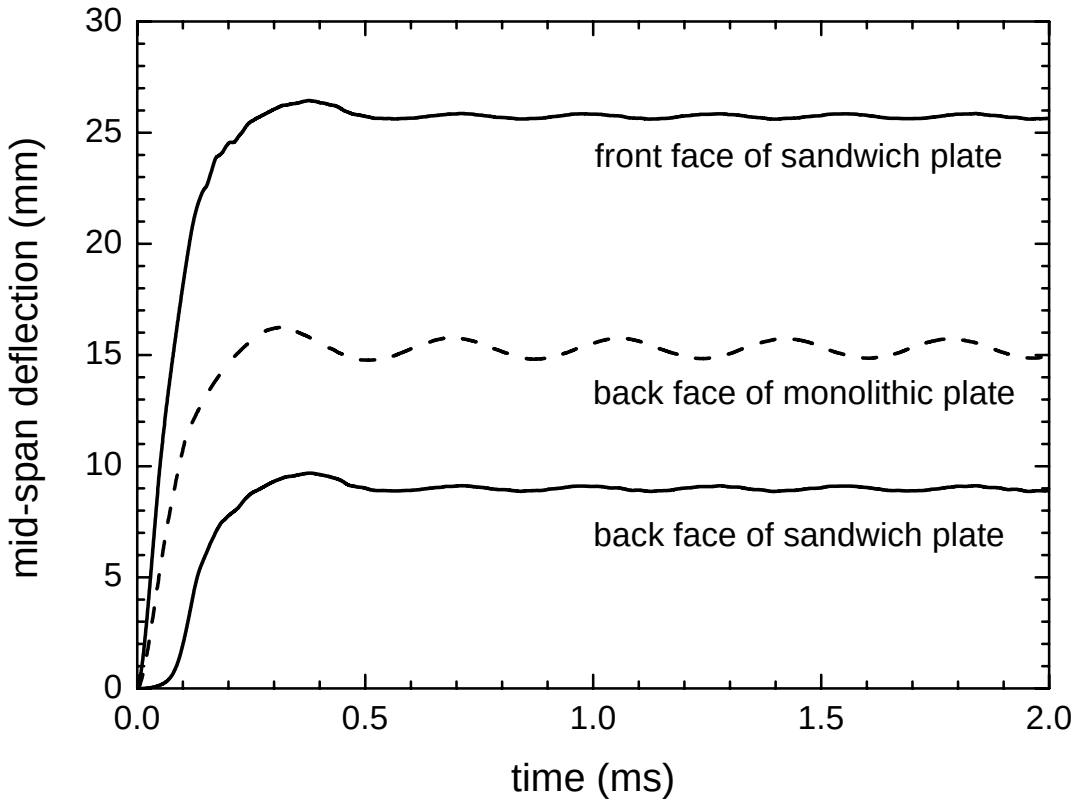

Figure 9. Finite element predictions of the mid-span deflection versus time histories of monolithic plate specimen M9 and $c = 22$ mm sandwich plate specimen B4. The figure shows the mid-span deflection of the back-face of the monolithic plate, and of both faces of the sandwich plate. $I_0 = 13$ kNs m^{-2}.

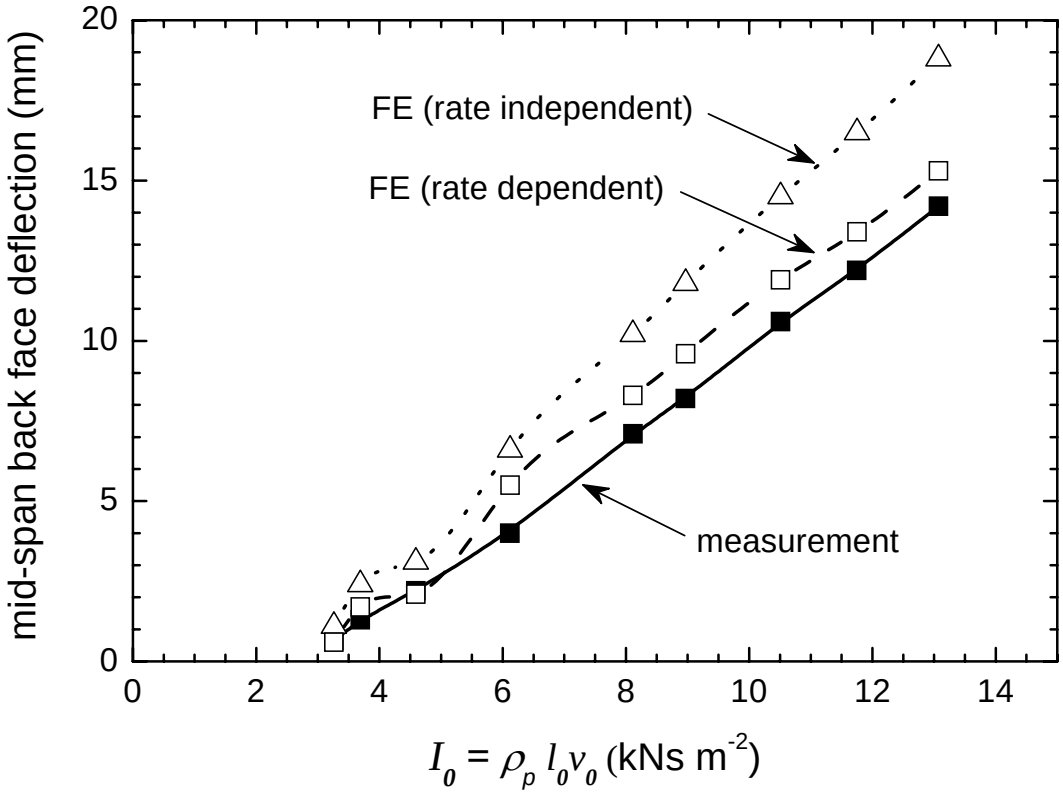

Figure 10: Measured and predicted back-face deflections for the monolithic plates.

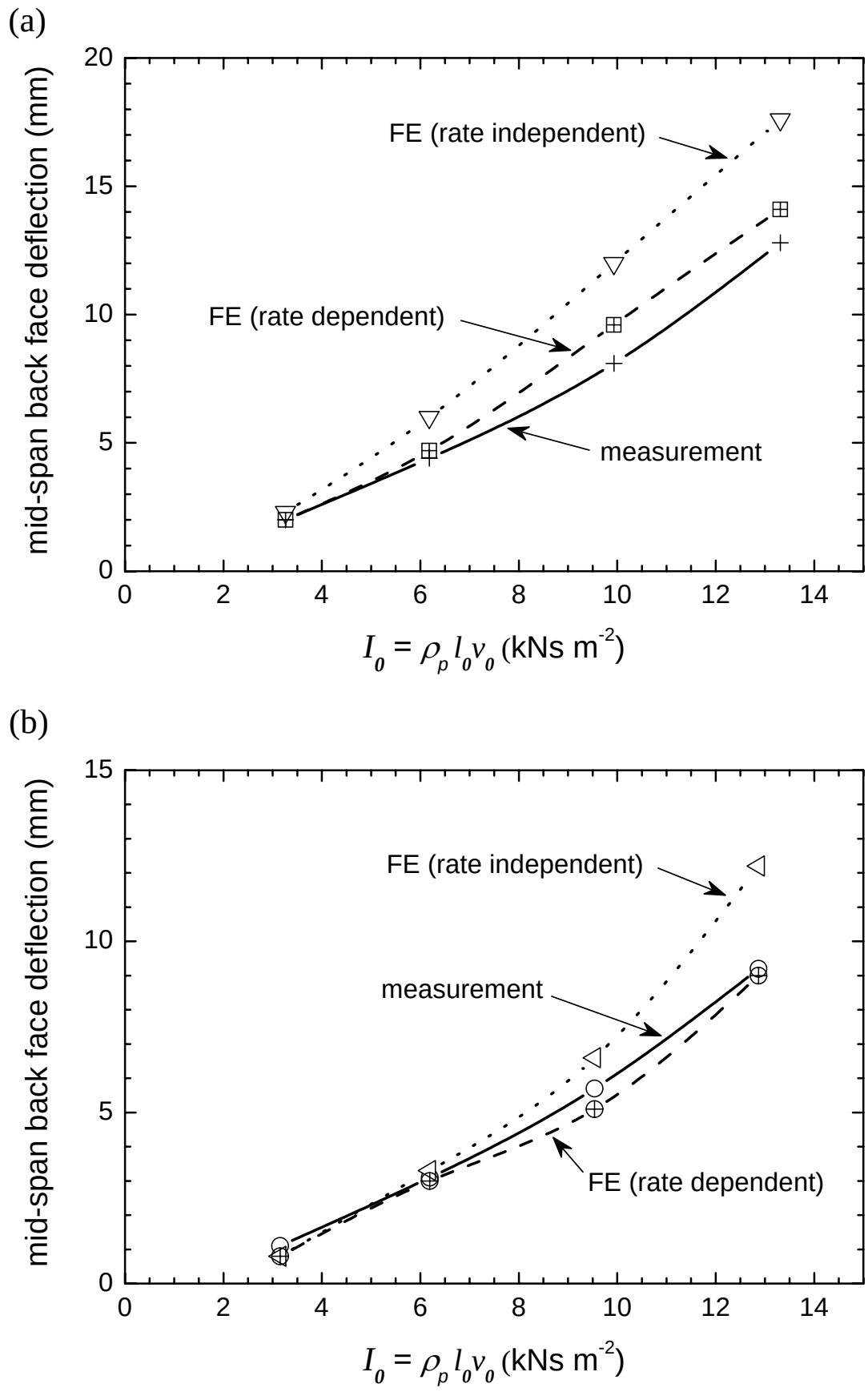

Figure 11. Measured and predicted back-face deflections for the (a) $c = 10$ mm and (b) $c = 22$ mm sandwich plates.

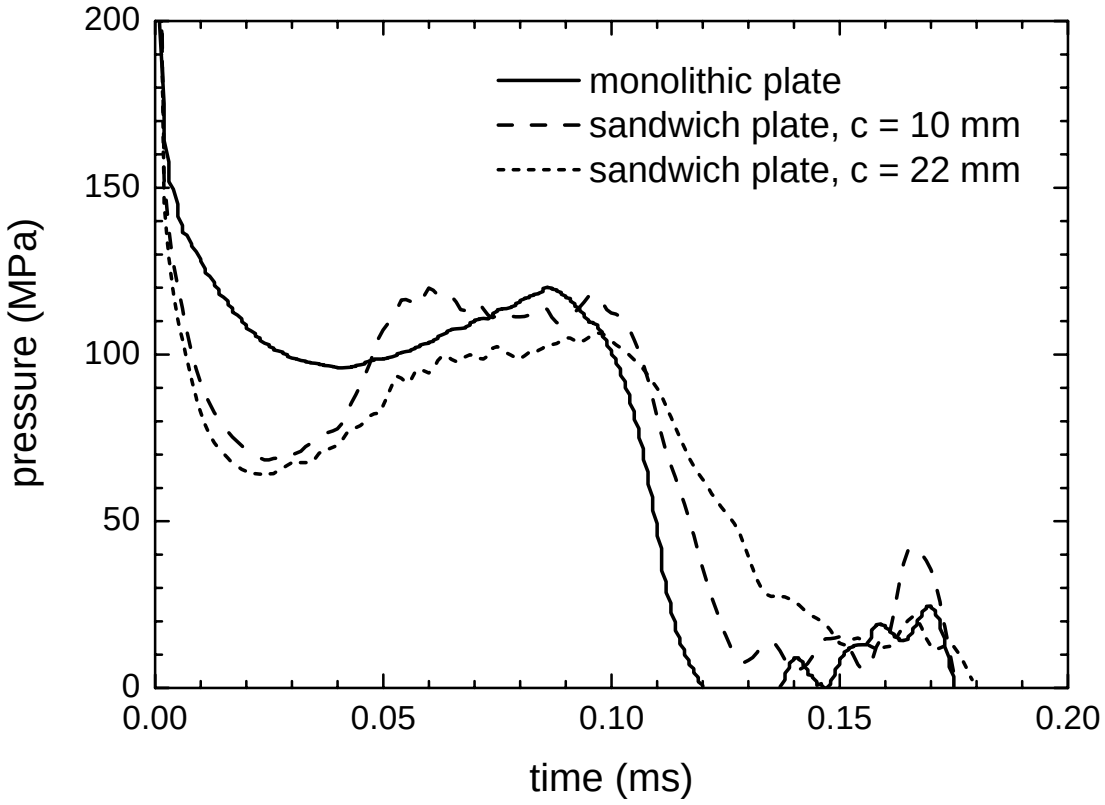

Figure 12. The predicted pressure versus time histories exerted by the foam projectiles on the monolithic specimen M9, and the sandwich plate specimens A4 ($c = 10$ mm) and B4 ($c = 22$ mm). $I_0 = 13$ kNs m^{-2}.

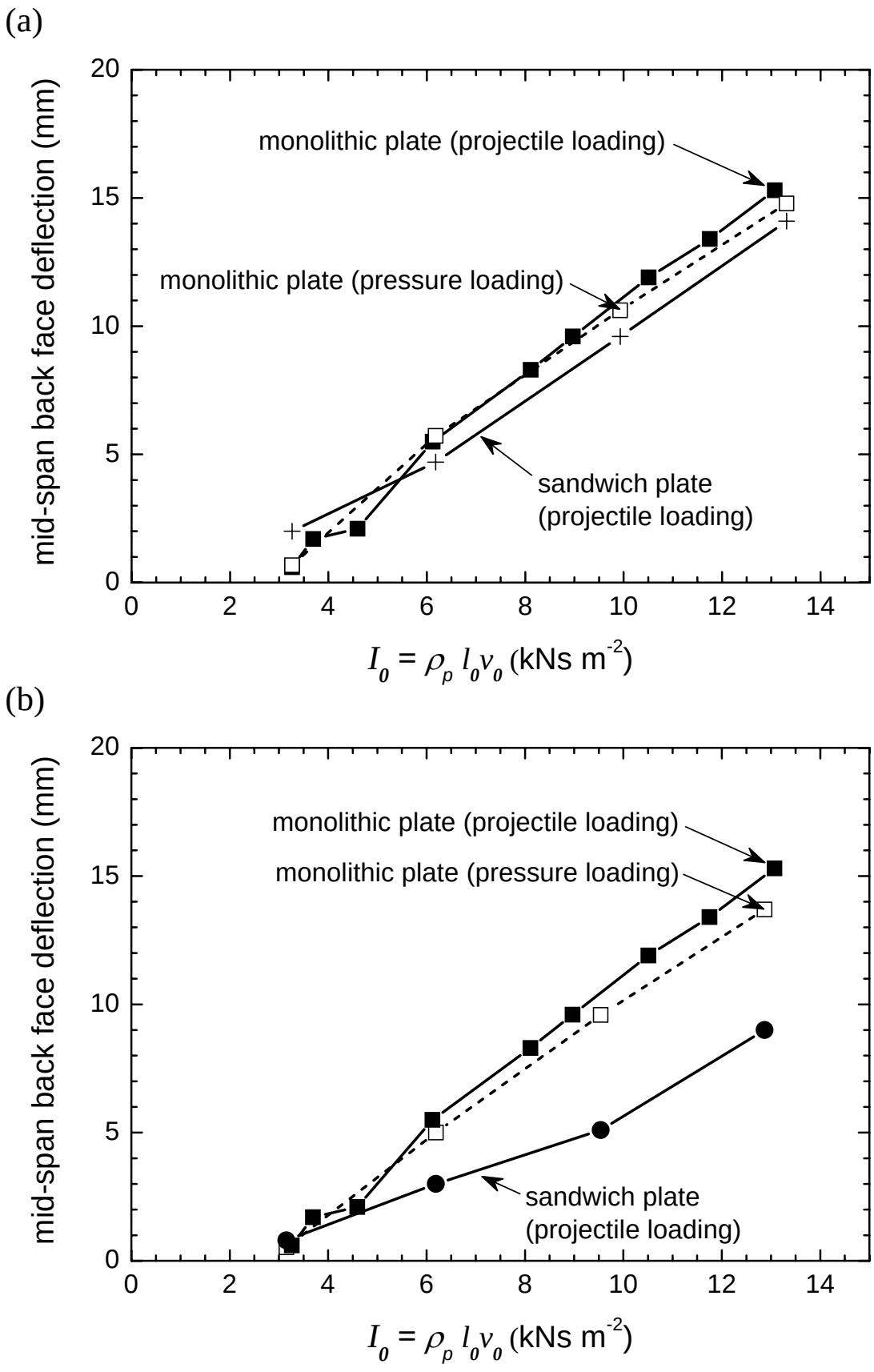

Figure 13: Predicted back-face deflections at mid-span. (a) Sandwich plate (c = 10mm) and monolithic plate loaded by projectile, and monolithic plate loaded by pressure transient. (b) Sandwich plate (c = 22mm) and monolithic plate loaded by projectile, and monolithic plate loaded by pressure transient.